Environmental Science & Technology

Article

Cite This: Environ. Sci. Technol. 2020, 54, 527−536

pubs.acs.org/est

Continuous Separation of Radionuclides from Contaminated Water by Shock Electrodialysis

Mohammad A. Alkhadra,[†,§] Kameron M. Conforti,[†,§] Tao Gao,[†] Huanhuan Tian,[†] and Martin Z. Bazant*[,†,‡]

[†]Department of Chemical Engineering and [‡]Department of Mathematics, Massachusetts Institute of Technology, Cambridge, Massachusetts 02139, United States

Supporting Information

ABSTRACT: The increasing popularity of nuclear energy necessitates development of new methods to treat water that becomes contaminated with radioactive substances. Because this polluted water comprises several dissolved species (not all of which are radioactive), selective accumulation of the radionuclides is desirable to minimize the volume of nuclear waste and to facilitate its containment or disposal. In this article, we use shock electrodialysis to selectively, continuously, and efficiently remove cobalt and cesium from a feed of dissolved lithium, cobalt, cesium, and boric acid. This formulation models the contaminated water commonly found in light-water reactors and in other nuclear processes. In a three-pass process, a consistent trade-off is observed between the recovery of decontaminated water and the percentage of cobalt removed, which offers flexibility in operating the system. For example, 99.5% of cobalt can be removed with a water recovery of 43%, but up to 66% of the water can be recovered if deionization of cobalt is allowed to drop to 98.3%. In general, the energy consumed during this process (ranging between 1.76 and 4.8 kW h m^{-3}) is low because only charged species are targeted and virtually no energy is expended removing boric acid, the most abundant species in solution.

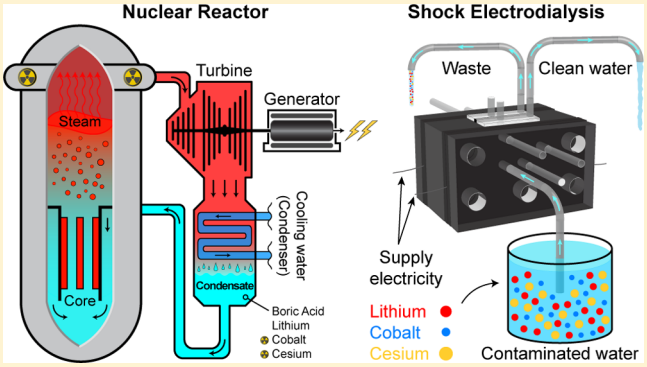

1. INTRODUCTION

Nuclear waste is matter that undergoes radioactive decay, a spontaneous process by which an unstable atomic nucleus emits radiation and concomitantly transforms into smaller daughter nuclei.[1] Although radioactive decay is stochastic at the level of individual nuclei, the expected rate of decay for a collection of radionuclides can be characterized in terms of an observable decay constant such as the half life.[1] Radioactive waste is often a byproduct in the industrial generation of nuclear power and is hazardous to the environment and to nearly all forms of life. Indeed, high-energy radiation can ionize atoms or even generate free radicals (e.g., hydroxyl from radiolysis of water) that react with the cellular components of an organism, which may cause aberration of chromosomes, mutation of nucleic acids, or death of cells.[2,3] Given the harmful nature of such radiation, the scientific community has sought to develop methods to isolate, manage, and dispose of nuclear waste. In this article, we adapt an emerging electrokinetic deionization method known as shock electrodialysis (SED)[4−8] to continuously treat water contaminated with radioactive ions. This study focuses on the basic physics and design principles needed to selectively remove cobalt (^{59}Co) and cesium (^{133}Cs), while recovering a reasonable fraction of the water fed and minimizing the energy cost of the process. Because SED is an electrokinetic method, separation of ions is based primarily on the charge and is insensitive to mass,[4,5] which implies that our results should also be applicable to radioactive isotopes of cobalt and cesium. The principal aim of our methodology is to concentrate nuclear waste in a contained discharge stream and, in turn, minimize the volume of waste that would need management, recycling, or disposal in subsequent processes.

Our strategy for separation is based on the phenomenon of deionization shock waves[9] by which a sharp gradient in the concentration of salt propagates near an ion-selective surface, such as a cation exchange membrane (CEMs)[4,5] or a metal electrodeposit.[10,11] Moreover, our system comprises a weakly charged porous medium to sustain overlimiting current—at which transport of ions is faster than by diffusion alone—as the conductivity of the solution diminishes near this surface.[5,10,12,13] The shock wave splits the system into a region that is concentrated and another that is deionized. These regions are then continuously separated by driving flow perpendicular to the applied electric field.[4] This system can therefore achieve electrically tunable and "membraneless"

Received: September 6, 2019
Revised: December 2, 2019
Accepted: December 3, 2019
Published: December 3, 2019

DOI: 10.1021/acs.est.9b05380
Environ. Sci. Technol. 2020, 54, 527−536

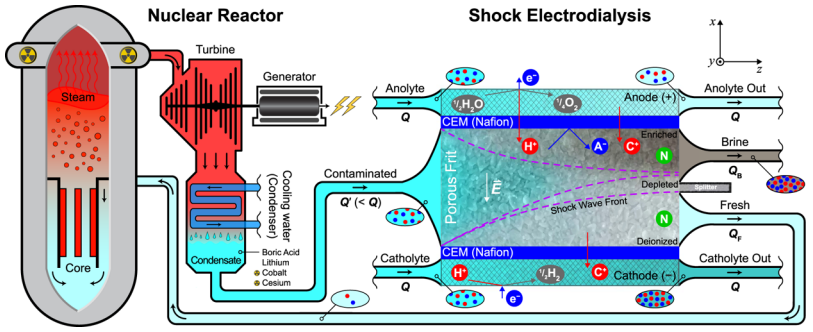

Figure 1. Operating principles of a light-water nuclear reactor and the SED device used for decontamination. (Left) Simplified schematic of a boiling water reactor [a type of light-water reactor (LWR)] used to generate electrical power by heating water that turns into steam and drives a turbine. Several radionuclides are present in this water and contaminate the reactor components outside the core; refer to 2 for details. (Right) Rectangular cross section of the SED device shows water splitting at the anode and formation of molecular hydrogen at the cathode (maintained under acidic conditions to prevent precipitation of metal hydroxides), which are the primary electrochemical reactions that provide current to the cell. Contaminated water in the frit is then subjected to an electric field ($\vec{E}$) that transports charged species (labeled C^+ for cations and A^- for anions) perpendicular to the flow. Anions are blocked by CEMs, and neutral species (labeled N) are unaffected by the electric field. Here, the flow rate is denoted by the letter Q, and streams are colored based on the relative concentration of ions.

separation within the porous material without any physical barriers in the direction of flow. In contrast to conventional electrodialysis in which the overlimiting current is often sustained by chemical or hydrodynamic instabilities,[14] overlimiting current in SED is sustained by electrokinetic phenomena at the scale of pores, namely surface conduction and electroosmosis.[5,12,13,15] Experimentally, concentration polarization was first observed in glass microchannels emanating from nanoscopic junctions[16−18] or membranes.[15] SED, however, relies on the propagation of macroscopic shock waves across a network of charged pores, which is necessary for flow fractionation,[5,7] scale-up to practical flow rates,[4] and improvement of both desalination[5,13] and water recovery (WR)[4] by leveraging electroosmotic flow.

The first laboratory scale prototype to successfully demonstrate SED was designed, built, tested, and patented by our group.[5−8] To achieve continuous operation, subsequent iterations of this system introduced a novel cross-flow architecture, in which the feed flows into a porous glass frit placed between identical CEMs, as shown in Figure 1.[4] The frit was made of sintered borosilicate glass, a porous material with negative charges bound to the surfaces of its pores, which were nominally 1 μm in size. By placing a splitter downstream of the frit, the exiting fluid was separated into enriched and deionized streams on the anodic and cathodic sides of the shock wave, respectively. Previous work showed that SED can continuously deionize electrolytes comprising monovalent cations, including NaCl, KCl, KNO_3, and Na_2SO_4.[4] (These measurements were made by quantifying changes in electrical conductivity of the solution). This work also revealed that WR (defined as the fraction of fluid recovered as desalinated water from the concentrated feed) can be increased to over 80% by increasing the applied current and without repositioning the splitter. Improved WR was attributed to electroosmotic flow perpendicular to the imposed flow, which conveniently delivered more fluid to the depleted region.

The present study is motivated by the recently discovered capability of SED to separate specific ions from multicomponent electrolytes. In particular, recent work demonstrated selective removal of magnesium—a divalent cation—from an aqueous mixture of NaCl and $MgCl_2$ with (retention) selectivity of up to 200:1 in the extreme case.[19] Because many radionuclides and harmful products of corrosion are present in water as multivalent ions, this result suggests that SED can be used to purify water contaminated with radioactive ions and byproducts of various nuclear processes.

2. BACKGROUND AND EXPERIMENTAL DESIGN

In treating radioactive water, the goal is often to separate the fluid into two streams. The first of these has low enough activity for safe discharge into the environment, and the second (with the smallest possible volume) is concentrated in radionuclides for further management. Existing methods for treatment can be broadly categorized into physical methods, which focus on extracting uncontaminated water, and chemical methods, which focus on extracting radionuclides. Physical methods include evaporation, reverse osmosis, nanofiltration, ultrafiltration, and microfiltration.[20−23] In these methods, water is driven across an interface (either a membrane or a gas−liquid interface in the case of evaporation) that retains dissolved species in a concentrated brine. The inclusion of an excess of boric acid (commonly done in the process water of various nuclear reactors for neutron poisoning[24,25]) complicates the use of several physical methods and makes them more energy intensive. This radioactively inert salt increases the osmotic pressure in membrane technologies such as reverse osmosis and is highly corrosive[26] when concentrated. For these reasons, selective removal is preferable to indiscriminately concentrating all dissolved species.[27]

Chemical methods, which are typically (but not always) selective in molecular separations, include solvent extraction (using liquid phase compounds), precipitation, chelation, ion exchange, and electrodeionization (EDI, sometimes called hybrid ion-exchange electrodialysis).[21,22] These methods target ions based on chemical reactivity (adsorption, chelation, and precipitation),[28,29] solubility and partition coefficient (solvent extraction),[30] affinity for charged or functionalized surfaces (ion exchange, EDI),[31−33] or response to electric fields in solution (EDI).[32] Apart from SED, EDI is the only technology that involves electrochemistry, and is the only chemical method that can operate continuously without the need for additives or solvents.[32] The remaining methods require the use of sacrificial chemicals, such as carriers or additives (adsorption, chelation, and precipitation), nonaqueous solvents (solvent extraction), or ion-exchange resins with

DOI: 10.1021/acs.est.9b05380
Environ. Sci. Technol. 2020, 54, 527−536

regenerating acids and salts (ion exchange), the disposal of which has been deemed challenging.[31,34]

In LWRs (see Figure 1 for a simplified schematic), the most common and active byproducts include cobalt-60 and cesium-137.[35,36] Cobalt-60 is the main contributor to high levels of radiation because it has a short half life (5.3 years) and emits high-energy gamma rays (1.17 and 1.33 MeV).[35] Cesium-137, on the other hand, has a longer half life (30 years) and is not as active as cobalt-60 but it is one of most abundant radionuclides produced from fission of uranium-235.[36,37] Moreover, this species poses long-term risks because, like cobalt-60, it produces high-energy beta particles and gamma rays.[38] Cesium in general is an alkaline metal that becomes a monovalent ion in solution and is chemically similar to sodium and potassium. Radioactive cesium is therefore readily taken up by biological organisms, in which it can deposit on soft tissue and, over time, induce thyroid cancer.[36] Compared to other radionuclides, cesium-137 has been deemed difficult to remove because of its small radius of hydration and high (mass) diffusivity.[36]

In this study, we prepared model radioactive water (referred to hereafter as "practical water") with the composition outlined in Table 1, as proposed by our sponsor, Mitsubishi Heavy Industries. This solution includes nonradioactive isotopes of the ions most abundant and active in the process water of LWRs, namely cobalt and cesium.[35,36] Boric acid is included abundantly as it is often used as neutron poison in these reactors because boron-10 can reduce the likelihood of thermal fission by absorbing neutrons.[24] Last, lithium-7 is used (in the form of LiOH) as an additive to control water chemistry and minimize the corrosive effects of boric acid.[39,40] During operation, small amounts of hazardous corrosion and fission byproducts (e.g., cobalt and cesium) are released into the process water, such that nonradioactive species may undergo radioactivation near the hot reactor core.[36,41−43] (e.g., cobalt-60 is produced when its precursor, cobalt-59, is bombarded with thermal neutrons; cobalt-59 is the naturally occurring isotope of cobalt with 100% abundance, and it is used in alloys that are required to possess thermal and mechanical resilience[44]). These species are then able to settle onto surfaces of the cooling system and recirculation pipes, and the quantity of undesired deposits of radionuclides increases with time.[41,45] Accumulation of radioactive matter in the structural portions of nuclear reactors is thus an occupational hazard to those who work in the vicinity of these systems and are exposed to such radiation. We note, however, that demineralization of process water in LWRs is only one possible application of SED, and the study of selective removal of cobalt and cesium is generally relevant to treatment of nuclear (waste)water.[20,21,46,47]

Table 1. Concentrations of Prevalent Species in Practical Water, the Nonradioactive Analog of Contaminated Process Water in Nuclear Reactors

species	concentration (ppm [mM])	role
boron	4000 [370]	present in boric acid; boron-10 serves as neutron poison[24]
lithium-7	2.2 [0.32]	used (as LiOH) to stabilize pH and control corrosion[39]
cobalt-59	20 [0.34]	cobalt-60 is the main contributor to high levels of radiation[35]
cesium-133	100 [0.75]	cesium-137 is one of the most abundant fission byproducts[36]

3. MATERIALS AND EXPERIMENTAL METHODS

The device used here was based on a design recently published by our group.[19] This continuous, laboratory scale architecture is illustrated in Figure 2. Our device included three inlets, two to transport fluid to the electrodes and a third to deliver contaminated feed, and four outlets, two to transport fluid from the electrodes and the other two to generate fresh and brine streams at the splitter. All fluids were transported through 1/8th in. Tygon tubing (Saint-Gobain) glued onto portplates made of cast acrylic. These portplates were used to seal liquids inside the device and to support the rubber tubing in which fluid flows. Moreover, four 1/16th in. Viton rubber gaskets (DuPont) were used to conformally seal the device and simultaneously provide channels for the electrode solutions

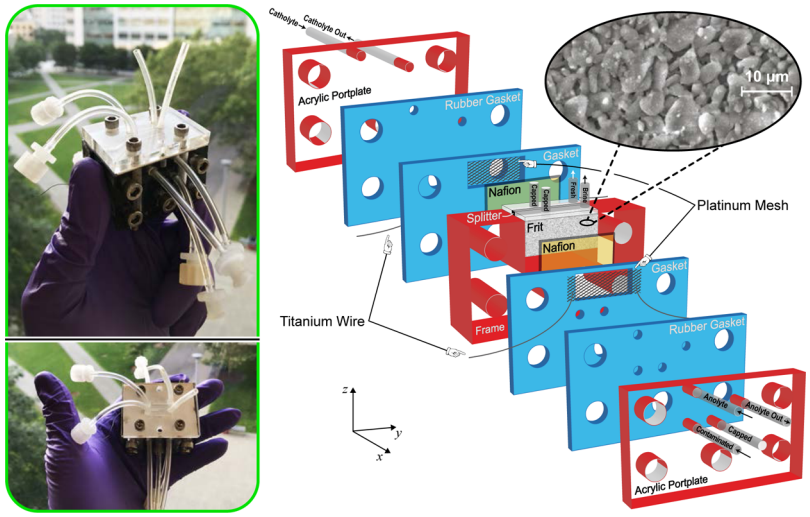

Figure 2. Photographs and 3D illustration of the SED device that shows assembly. Working device consists of platinum electrodes, titanium wire, and a microporous borosilicate frit sandwiched between identical Nafion membranes which permit passage of only cations. Inlet (outlet) streams are labeled contaminated, anolyte (anolyte out), and catholyte (catholyte out); fluid leaving the top edge of the frit is split into *fresh* and *brine* streams. Close-up image of a glass frit was taken by scanning electron microscopy.

DOI: 10.1021/acs.est.9b05380
Environ. Sci. Technol. 2020, 54, 527−536

(catholyte and anolyte). The electrodes in this device were platinum meshes (Sigma-Aldrich) that were connected to a Gamry Reference 3000 potentiostat/galvanostat using titanium wires (Alfa Aesar). The electrodes and wires were secured in place by compressible Viton gaskets. CEMs (Nafion N115, Ion Power) with a thickness of approximately 130 μm served as fluidic barriers between the electrode channels and the porous medium, which in this study was a borosilicate frit (Adams & Chittenden Scientific Glass) with ultrafine pores (nominally ranging from 0.9 to 1.4 μm in size), an internal surface area of 1.75 $m^2\ g^{-1}$ based on Brunauer–Emmett–Teller theory, a mass density of 1.02 g m^{-3}, a porosity of 0.31, and dimensions of 0.9 cm × 2 cm × 1 cm. Prior to assembly, the frit was glued onto an acrylic frame using Devcon 2 Ton Epoxy (McMaster-Carr). The splitter (placed midway down the frit for ease of assembly) was made of cast acrylic and was sealed against the top face of the frit using the 0.04 in. GORE expanded polytetrafluoroethylene gasket tape. Holes in all of the acrylic slabs and rubber gaskets were formed using a laser cutter (Universal Laser Systems) and refined with a drill press (Palmgren 10 in., 5-speed bench model). These layers were then stacked and held together with nuts, bolts, and washers made of 316 stainless steel.

To prepare practical water with the composition shown in Table 1, we formulated stock solutions with 1000 times the target concentrations made from lithium hydroxide monohydrate ($LiOH{\cdot}H_2O$), cobalt(II) chloride hexahydrate ($CoCl_2{\cdot}6H_2O$), and cesium chloride (CsCl). Appropriate volumes of these solutions were then diluted in deionized water, followed by the addition of solid boric acid (H_3BO_3) to achieve a concentration of 370 mM. (All reagents were purchased from Sigma-Aldrich and used as received). We note that H_3BO_3 is a weak acid with a first pK_a of 9.24 in pure water at room temperature. With the following equation for dissociation equilibrium

$$H_3BO_3 \rightleftharpoons H^+ + H_2BO_3^- \tag{1}$$

we determined the concentration of $H_2BO_3^-$ to be approximately 0.015 mM in solution. This weak dissociation implied that virtually all of the boron was present as electrically neutral boric acid and thus was not separated by SED. We recognized, however, that H_3BO_3 could have influenced the pH of practical water, the dynamics of proton transport, and the extent of ionic separation. The pH of practical water (assumed here to be an ideal solution) was indeed calculated assuming partial dissociation of H_3BO_3 and complete dissociation of LiOH. By definition of the equilibrium constant K_a, we obtained

$$\frac{[H^+][H_2BO_3^-]}{[H_3BO_3]} = K_a = 10^{-pK_a}$$
$$\Rightarrow \frac{[H^+]([LiOH]_0 + [H^+])}{[H_3BO_3]_0 - [LiOH]_0 - [H^+]} = 10^{-pK_a} \tag{2}$$

where brackets denote concentration (molarity), $[H_3BO_3]_0$ = 0.37 M, $[LiOH]_0$ = 0.32 mM, and pK_a = 9.24. Solving this algebraic equation gave

$$[H^+] = 6.6 \times 10^{-7}\ M \Rightarrow pH = -\log([H^+]) = 6.2 \tag{3}$$

In preparing practical water, the anolyte and contaminated feed were identical in composition, whereas the catholyte included an additional dose of hydrochloric acid (HCl) with a concentration of 10 mM. This dose of HCl was deliberately added to prevent precipitation of cobalt hydroxide that could have formed as a result of hydrogen evolution in the otherwise basic catholyte.

With these solutions prepared, experiments began by setting the flow rates of all streams. In this report, all flow rates were held constant: 0.21 ± 0.01 mL min^{-1} for the electrode streams (anolyte and catholyte) and 0.065 ± 0.003 mL min^{-1} for the contaminated feed. To transport these streams to the SED device, we used peristaltic pumps equipped with Tygon Chemical tubing (Saint-Gobain). With such pumps—and at low speeds of rotation—the flow would be pulsed, though it was made smooth by incorporating a small buffering tank known commonly as a hydraulic accumulator (or capacitor) just upstream of the device. In our design, the accumulators were capped glass vials that held a small volume of (compressible) air above the (incompressible) liquids being pumped at the bottom to smooth out pulsations. With flow rates set and tubing connected, the accumulators were left to pressurize and the system to equilibrate overnight, after which the Gamry was set to operate in galvanostatic mode. (Air inside the accumulators became pressurized over time until the fluidic resistance downstream—such as that created by the porous frit—was overcome by the pumped liquid). The measured voltage was allowed to stabilize for at least 1 h until it reached steady state.

Samples were collected directly from the device in graduated cylinders and stored in conical centrifuge tubes for analysis, which included measurement of volume, conductivity, pH, and composition of cations. Conductivity and pH were measured using Mettler Toledo analytical instruments (SevenCompact pH/Cond S213), and composition was determined using inductively coupled plasma mass spectrometry (Agilent 7900 ICP–MS). The plasma in ICP–MS was made from argon gas and was supplemented by helium, which is normally needed to analyze elements with high ionization energies (e.g., Co) for which argon plasma alone is not a sufficient source of ionization.[48] To improve the accuracy of our data and subsequent analysis, we incorporated an internal standard that introduced 100 ppb of indium to all of our samples. Because the output of ICP–MS was numerical (in counts per second), quantitative analysis required calibration of the measurements, which was achieved by processing a set of reference standards and producing a calibration curve, an example of which is shown in Figure S1 (Supporting Information). These standards (Li, Co, Cs, and In) were purchased from Sigma-Aldrich and serially diluted to prepare a set of samples encompassing the concentrations relevant to this study. All samples and standard solutions were diluted in 2 vol % nitric acid prior to analysis by ICP–MS.

4. RESULTS AND DISCUSSION

4.1. Principles and Performance of SED. The key phenomenon that governs deionization in SED is propagation of a shock wave across which concentration varies drastically and a depletion zone is formed. This shock is generated by providing the system with an overlimiting current, which is current in excess of the flow-limited current (I_{lim}) defined as

$$I_{lim} = \sum_k \nu_k C_k F Q' \tag{4}$$

where ν is valence (charge), C is molar concentration, F is Faraday's constant, Q' is the volumetric flow rate of the feed,

DOI: 10.1021/acs.est.9b05380
Environ. Sci. Technol. 2020, 54, 527–536

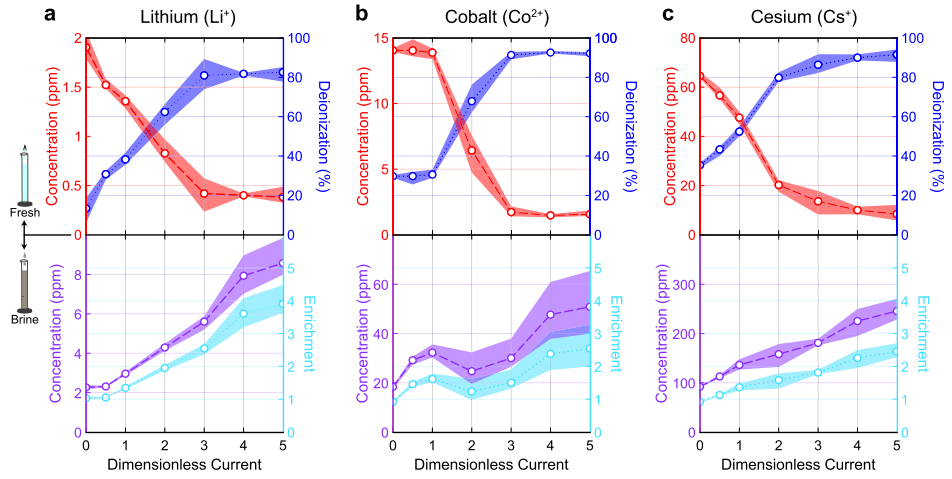

Figure 3. Quantitative analysis of the deionization of (a) lithium, (b) cobalt, and (c) cesium in practical water. Upper (lower) half of each panel shows the measured concentration and calculated deionization (enrichment) in the fresh (brine) stream as functions of dimensionless current. Concentration of ions in the feed was 1.41 mM, with compositions outlined in Table 1. Each data point represents the arithmetic mean of four samples, and the shaded areas correspond to the range of those samples.

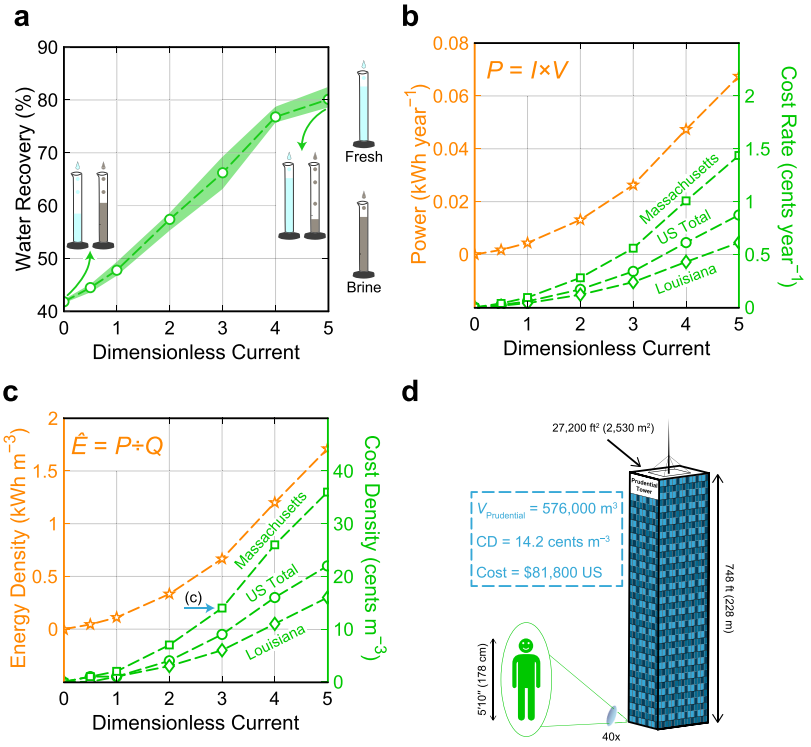

Figure 4. Quantitative analysis of the WR and energy demand/cost corresponding to the results shown in Figure 3. (a) WR as a function of dimensionless current; graduated cylinders portray relative proportions of the fresh and brine products, and each data point represents the arithmetic mean of four samples with the shaded area corresponding to the range of those samples. (b) Power and cost rate as well as (c) energy density and cost density as functions of dimensionless current; cost rate (cost density) is equal to power (energy density) multiplied by the residential cost of electricity, which varies between states in the US. (d) Cartoon schematic to aid with visualization of the cost needed to apply three times the dimensionless current to a body of water with volume equal to that of the Prudential Tower in Boston, MA; CD is cost density from (c).

and the sum is taken over all cations k. This definition of I_{lim} can be interpreted as the rate of forced convection of positive charge carriers into the device, and it was assumed that the flux of anions is 0 at steady state in the presence of ideal CEMs. Using the composition of practical water in Table 1 and with $Q' = 0.065$ mL min^{-1}, we found that $I_{lim} = 180$ μA. We verified this value experimentally by performing a conventional voltage sweep from 0 to 10 V and measuring the current, as shown by the $I-V$ curve in Figure S2 (Supporting Information). After exceeding I_{lim}, the (overlimiting) current increased linearly with voltage and effected constant conductance, which was consistent with the governing theory and previous experimental observations in negatively charged porous media.[4,12]

Based on a previous study by our group, we operated our SED system in galvanostatic mode (see Figure S3 in the Supporting Information) because it facilitates the formation of

DOI: 10.1021/acs.est.9b05380
Environ. Sci. Technol. 2020, 54, 527−536

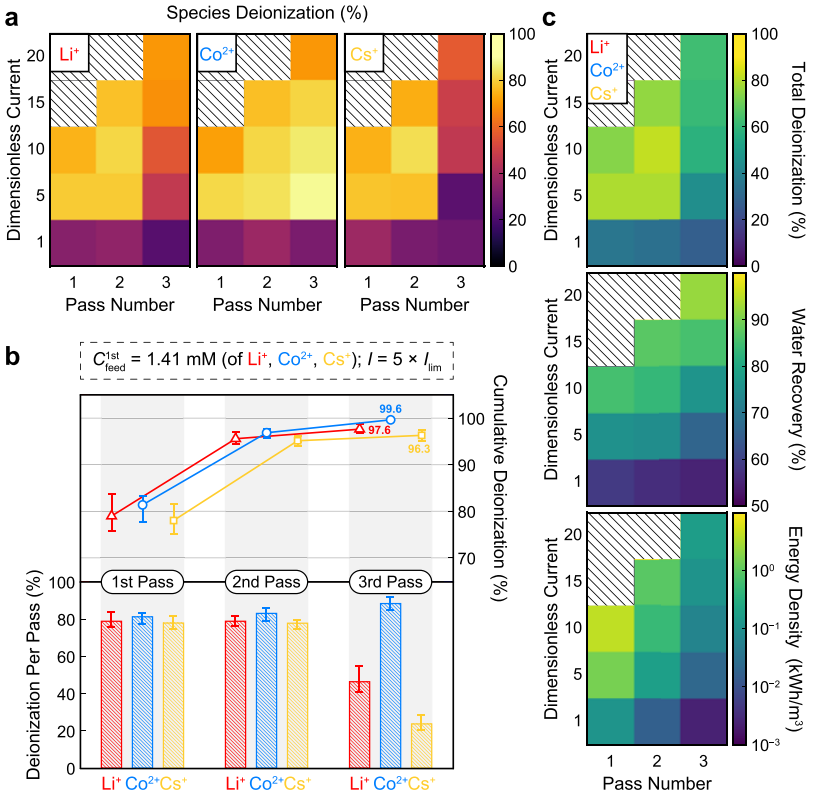

Figure 5. Simulation of a 3-step process for deionization of practical water by feeding serially diluted solutions in turn to the same device; neglecting boric acid, concentrations of the feed to each pass were 1.41 mM (I_{lim} = 180 μA), 0.282 mM (5× dilution, I_{lim} = 36μA), and 0.0564 mM (25× dilution, I_{lim} = 7.2 μA), respectively. (a) Two-dimensional array of deionization as a function of dimensionless current in each pass. (b) Deionization per pass (bottom) and cumulative deionization (top) for each species with a dimensionless current of 5; each data point represents the arithmetic mean of three samples with errors bars corresponding to the range of those samples. (c) Two-dimensional arrays of total deionization (top) for the three target species, WR (middle), and energy density (bottom) as functions of dimensionless current in each pass. Zones of diagonal black stripes in (a) and (c) correspond to parameters that were not tested.

a stable deionization shock wave when supplying overlimiting current.[4] (Potentiostatic operation, on the other hand, tends to result in overshoot and oscillation about a desired overlimiting current and is associated with variability in the shock wave[17]). Our results for treatment of practical water are presented in Figure 3, where deionization (the percentage removed of a given species, DI) is defined as

$$\mathrm{DI} = 100\% \times \left(1 - \frac{C_{\mathrm{fresh}}}{C_{\mathrm{feed}}}\right) \tag{5}$$

enrichment factor (EF) as

$$\mathrm{EF} = \frac{C_{\mathrm{brine}}}{C_{\mathrm{feed}}} \tag{6}$$

and dimensionless current ($\tilde{I}$) as $\tilde{I} = I/I_{\mathrm{lim}}$. The upper half of this figure illustrates that the concentration of cations (Li^+, Co^{2+}, and Cs^+) in the fresh stream decreased—by up to 92% for both Co^{2+} and Cs^+—with current. Moreover, the lower half shows that the concentration of cations in the brine stream increased with current. Deionization that occurred with no applied current was most likely due to exchange of H^+ (abundant in the cathode) with cations in practical water across the lower membrane.

4.2. WR and Energy Cost. Given the importance of WR and energy efficiency in desalination systems, we analyzed the recovery ability and energy demand of SED when used to treat practical water. WR, sometimes referred to the recovery ratio, is defined as

$$\mathrm{WR} = \frac{Q_{\mathrm{F}}}{Q'} \tag{7}$$

where Q_F is the volumetric flow rate of the fresh stream, and it is shown in Figure 4a to increase (up to 80%) with current. This increase in WR is predominantly due to electroosmotic flow (see Figure 3d and the Supporting Information in ref 4); the position of the splitter was not changed in this study, although it could be adjusted in future designs for improved WR. Analysis of the electrical energy needed for deionization is shown in Figure 4b,c, where power P is the product of applied current and (steady) voltage, and energy density $\hat{E}$ is power divided by the volumetric flow rate of the feed. Although electrical power is the more natural measure of energy transport, it is extensive and does not scale with the size of a system (particularly with flow rate). Energy density is therefore of greater value in quantifying the energy efficiency of SED. In treating practical water, the energy density increases quadratically with current, though it was on the order of 1 kW h m^{-3} for dimensionless currents between 3 and 5. Moreover, the cost of fluidic pumping in our laboratory scale system was negligible compared to the cost of electrical energy:

DOI: 10.1021/acs.est.9b05380
Environ. Sci. Technol. 2020, 54, 527−536

$$P_{pump} = N[Q'\Delta p_{frit} + Q(\Delta p_{anoylte} + \Delta p_{catholyte})] = 2.0 \times 10^{-3}\ \text{kW h year}^{-1}$$

$$\hat{E}_{pump} = N[\hat{E}_{frit} + \hat{E}_{anolyte} + \hat{E}_{catholyte}] = 4.2 \times 10^{-2}\ \text{kW h m}^{-3} \quad (8)$$

where N is the number of passes (3 here), Δp is pressure drop (6.1 psi across the frit and 0.67 psi across each of the electrodes), and $Q = 0.21$ mL min^{-1} is the volumetric flow rate of the electrode streams. At commercial scales, however, we expect that the cost of pumping will become important and will increase according to the desired level of throughput.

A more intuitive way of understanding the energy efficiency of SED is to consider the cost rate (Figure 4b) or cost density (Figure 4c), which are equal to power or energy density, respectively, multiplied by the cost of residential electricity per kilowatt hour. We present average electricity data for a state in which electricity is expensive (MA, \$0.21 kW h^{-1}) and in the other cheap (LA, \$0.09 kW h^{-1}) relative to the US total (\$0.13 kW h^{-1}); costs are based on 2018 data gathered from the US Energy Information Administration (EIA).[49] Figure 4d is a cartoon that helps visualize the cost needed to apply three times the dimensionless current (enough to remove 82% of Li^+, 91% of Co^{2+}, and 85% of Cs^+) to a body of water with a volume equal to that of the Prudential Tower in Boston, MA. For comparison, a nuclear reactor with an electrical power output of 1.7 GWe, such as the US Advanced Pressurized Water Reactor, requires coolant at a flow rate of approximately 28 m^3 s^{-1}.[50] This flow rate corresponds to 8.8×10^8 m^3 (>1500 times the volume of the Prudential Tower) of water that passes through the reactor core annually. The simple economic analysis introduced here will be useful when SED is being scaled up for use at commercial scale.

4.3. Implementation of a Multistep Process. For common desalination technologies, performance is improved and energy consumption is reduced by using multiple units or stages of the technology in series and by operating each stage at lower power.[51,52] Such an approach is especially suitable for SED because power increases quadratically with current (Figure 4), even though deionization eventually plateaus (Figure 3).[53] To demonstrate this claim, we developed a new configuration for our system that involved a 3-step process for deionization of practical water. Because the throughput of our laboratory scale device was low, we accelerated experimentation with this process by feeding serially diluted solutions in turn to the same device. A dilution factor of 5 was chosen for the second step and 25 for the third based on deionization of the target species in the first two steps at a dimensionless current of 5. In other words, concentrations of the feed to each pass were 1.41, 0.282, and 0.0564 mM, neglecting boric acid. In Figure 5a, we present two-dimensional arrays of deionization for each species as a function of dimensionless current in each pass. In these experiments, dimensionless current ranged from 1 to 20, though deionization typically plateaued at some intermediate value. To examine the performance of our system at one such value, we report deionization per pass and cumulative deionization for each species at a dimensionless current of 5, as shown in Figure 5b. In the first and second passes, all three species were removed in nearly equal proportions, whereas in the third pass, Co^{2+} was preferentially removed (see Figure S4 in the Supporting Information for discussion of this observation). This selective separation of the divalent ion agrees with a previous experimental study by our group, in which magnesium was selectively removed from an aqueous mixture of NaCl and $MgCl_2$.[19] Figure 5b also shows that our 3-step process led to a high cumulative deionization for each species, ranging from 96.3% for Cs^+ to 99.6% for Co^{2+}. Based on its ability to remove target ions from practical water, SED could function as a novel method for treatment of radioactive waste.

In addition to removal of target ions, effective methods for decontamination of water must also be optimized for total deionization, WR, and energy density. These quantities are shown for our 3-step process in Figure 5c and are consistent with the previously observed trends: total deionization often plateaus at some moderate value of dimensionless current, whereas WR and energy density increase monotonically with current. It is striking to learn that our device can sustain WR at over 92% ($\tilde{I} = 20$) primarily by electroosmotic flow[4] and even though the splitter is positioned midway along the width of the frit. Moreover, successive steps in this process contribute little energy in addition to that consumed in the first step (see Figure S3 in the Supporting Information), which implies that a contaminated feed can be repeatedly passed through the device for greater deionization at a reduced cost. This proportionality between energy demand and concentration of the feed—even in the dilute limit—gives SED an advantage over conventional purification techniques, which typically require an input of energy that is bounded from below as the feed becomes more dilute. As with other desalination methods, removal of more ions by multistep SED comes at the expense of water recovery, which diminishes in every pass. We will address this challenge in future generations of our device by introducing a recycle scheme that feeds the brine stream from a later pass back to an earlier pass the feed to which is of comparable concentration.

So far, we quantified the ability of SED to remove target species from practical water and identified general rules to optimize the design of a real system that can treat nuclear waste. In particular, we inferred a complex coupling between the extent of deionization—convoluted by the selective nature of separation by SED (Figure S4 in the Supporting Information)—WR, and energy demand. The relationship between these parameters is nonlinear, and indeed, we observe quadratic growth in energy density with applied current (Figures 4b,c and 5c). Moreover, deionization varies between species and is not monotonic, and WR appears to increase sublinearly with applied current (Figures 4a and 5c). These results suggest that there is an inherent trade-off between deionization, WR, and energy efficiency, which poses a significant challenge in satisfactorily treating nuclear waste while minimizing the demand for power. We addressed this challenge from the perspective of systems engineering by introducing a new figure of merit (Ψ) defined as

$$\Psi = \text{DI}^2 \times \text{WR}^n \times f(\hat{E}) \quad (9)$$

where DI is deionization (squared to emphasize this metric), WR is water recovery, n is a positive integer (either 1 or 2 here), and $f(\hat{E})$ is a dimensionless function of energy density that ranges from 0 to 1. This function may be constant

$$f(\hat{E}) = 1 \text{ (no penalty on energy demand)} \quad (10)$$

linear

DOI: 10.1021/acs.est.9b05380
Environ. Sci. Technol. 2020, 54, 527−536

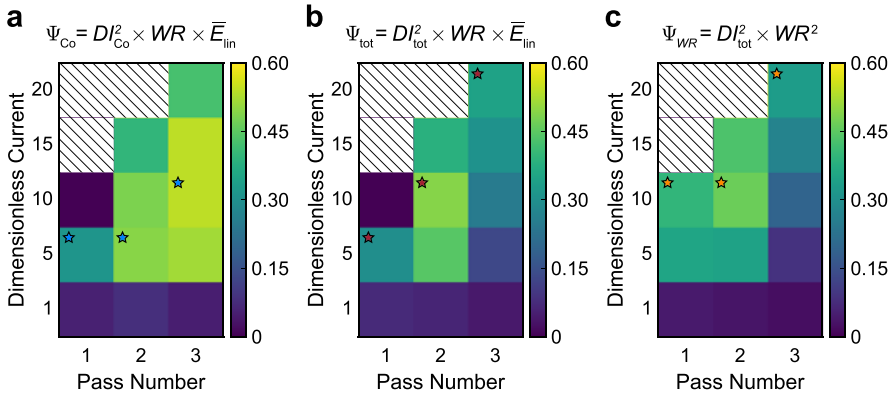

Figure 6. Quantitative characterization of the performance of the 3-step process shown in Figure 5. Figure of merit Ψ (as defined in eq 9) based on (a) deionization of cobalt only DI_{Co}, (b) total deionization DI_{tot}, and (c) WR (weighted quadratically, and with no penalty on energy demand) as functions of dimensionless current in each pass; light blue (a), dark red (b), and orange (c) stars indicate which steps in the sequence of passes maximize Ψ (see Table 2). Zones of diagonal black stripes in the upper left corners correspond to parameters that were not tested.

Table 2. Summary of Total (and Individual) Deionization, DI, Water Recovery, WR, and Energy Density, $\hat{E}$, for the Sequence of Passes that Maximizes the Figure of Merit Ψ in Figure 6 (Designated by Light Blue (a), Dark Red (b), and Orange (c) Stars)

	DI_{tot} (%)	DI_{Li} (%)	DI_{Co} (%)	DI_{Cs} (%)	WR (%)	$\hat{E}$ (kW h m^{-3})
optimal sequence for Ψ_{Co}	98.1 ± 0.2	98.0 ± 0.2	99.5 ± 0.1	97.3 ± 0.5	43 ± 2	1.76 ± 0.04
optimal sequence for Ψ_{tot}	98.6 ± 0.1	98.8 ± 0.2	98.9 ± 0.3	98.3 ± 0.2	58 ± 2	2.18 ± 0.05
optimal sequence for Ψ_{WR}	98.2 ± 0.2	98.5 ± 0.3	98.3 ± 0.4	98.1 ± 0.2	66 ± 2	4.8 ± 0.2

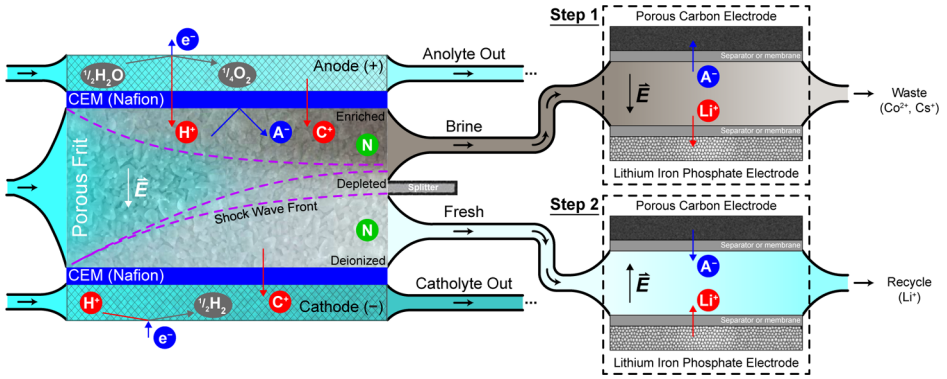

Figure 7. Process intensification of SED by using CDI to recycle Li^+ in two steps. First step involves selective capture of Li^+ in the CDI unit from the brine stream discharged by SED. Selectivity is achieved by intercalation of Li^+ into an iron phosphate electrode, which becomes lithium iron phosphate (Li_xFePO_4) upon insertion of Li^+. Second step involves the release of Li^+ into the fresh stream exiting the SED device by reversing the direction of electric field.

$$f(\hat{E}) = \bar{E}_{lin} \equiv 1 - \frac{\hat{E}}{\max \hat{E}} \tag{11}$$

or nonlinear with respect to $\hat{E}$

$$f(\hat{E}) = \bar{E}_{quad} \equiv \sqrt{\frac{1 - \hat{E}/\max \hat{E}}{1 - \min \hat{E}/\max \hat{E}}} \tag{12}$$

where "min" and "max" operate on the entire array of energy densities in Figure 5c. Although we only considered eqs 10 and 11 in this study, a nonlinear function such as eq 12 could be used to detract from the merit of steps that operate at high power, such that this penalty would become increasingly severe as $\hat{E}$ approaches max $\hat{E}$. In any case, all terms in the expression for Ψ (and hence Ψ itself) would range from 0 to 1.

Introducing a figure of merit allows us to quantitatively decide which operating conditions in each pass maximize deionization in our system. Characterization of the performance of our 3-step process is shown in Figure 6 based on several variations of Ψ. For example, Ψ may be based on deionization of cobalt only (Figure 6a) or total deionization (Figure 6b). These variations of Ψ, both with $n = 1$, suggest the same value of dimensionless current in only the first pass ($\tilde{I} = 5$) but suggest different values in the second and third passes (as designated by the colored stars). This difference can be rationalized by the fact that deionization of Co^{2+} (and not of Li^+ or Cs^+) is often greatest at low to moderate dimensionless current (Figure 5a).

To select the most suitable operating conditions, we compared total (and individual) deionization, WR, and energy density, all of which are summarized in Table 2, for the sequence of passes that maximizes the corresponding variation of Ψ. The sequence that maximizes Ψ_{Co} in each step, for instance, leads to relatively low WR, but the energy it consumes is also the least. In comparison, the sequence that

DOI: 10.1021/acs.est.9b05380
Environ. Sci. Technol. 2020, 54, 527−536

maximizes Ψ_{tot} in each step gives WR = 58%, and it maintains almost 99% deionization of Co^{2+} with little additional demand for energy. This level of water recovery is similar to those achieved by conventional purification technologies, though it can be increased by selecting an alternate sequence in our process. To make a quantitatively motivated selection, more weight is given to WR by setting $n = 2$ and $f(\hat{E}) = 1$ in our definition of Ψ, as shown in Figure 6c. With this modification, the sequence that maximizes Ψ_{WR} in each step gives WR = 58%. In response, however, consumption of energy increases considerably. It then seems that WR can be improved in return for higher energy consumption (or lower deionization, by repositioning the splitter) depending on the targets set by the operator.

4.4. Process Intensification for Lithium Recovery. For all cases shown in Table 2, total deionization is approximately 98%, and deionization of Co^{2+} is even greater in our 3-step process. Another practical result is the high deionization of Li^+, which is used (as LiOH) in nuclear reactors for corrosion control by alkalizing the process water.[39] For this application, LiOH is isotopically enriched in lithium-7 which does not interfere with nuclear reactions (unlike lithium-6), and it is sometimes used in demineralizers (also known as ion exchangers) to remove radioactive contaminants from the process water.[54] Lithium can be selectively captured and recycled in our system (or reused elsewhere) by integrating capacitive deionization (CDI) with intercalation materials[55,56] as a second operation following SED. This process intensification can in principle be achieved in two steps, as illustrated in Figure 7. In the first step, SED is used to concentrate waste in the brine stream, from which Li^+ is selectively captured in the CDI unit by intercalation into an appropriate electrode such as iron phosphate[57] ($Fe(III)PO_4$, often prepared by deintercalation of Li^+ from $LiFe(II)PO_4$) or lithium manganese oxide[58] ($LiMn_2O_4$). During this process, all cations are driven toward the intercalation electrode, but only Li^+ can be inserted into its crystal lattice because Cs^+ is too large and Co^{2+} will exhibit strong Coulomb repulsion (vacancies in $FePO_4$ are fitted for small monovalent cations[57]). Moreover, the anions are inserted into a porous carbon electrode, where they are electrostatically trapped by the applied potential. Fluid leaving the device in this first step will therefore be depleted of lithium and its counterion(s). In the second step, the fresh stream produced by SED is passed through the CDI unit. By reversing the direction of electric field, lithium and its counterion(s) are released from the electrodes back into solution and are recovered for later use.

■ ASSOCIATED CONTENT

Supporting Information

The Supporting Information is available free of charge at https://pubs.acs.org/doi/10.1021/acs.est.9b05380.

Representative calibration curve for ICP−MS, current and voltage data, analysis of species selectivity, and conductivity and pH data (PDF)

■ AUTHOR INFORMATION

Corresponding Author

*E-mail: bazant@mit.edu.

ORCID

Mohammad A. Alkhadra: 0000-0003-3866-709X

Martin Z. Bazant: 0000-0002-8200-4501

Author Contributions

§M.A.A. and K.M.C. have equal contribution.

Notes

The authors declare no competing financial interest.

■ ACKNOWLEDGMENTS

This research was supported by a grant from Mitsubishi Heavy Industries Limited. The authors thank the Center for Environmental Health Sciences (CEHS) at MIT for use of ICP−MS.

■ REFERENCES

(1) Giancolli, D. C. *Physics: Principles with Applications*, 6th ed.; Prentice Hall, 2005.

(2) Lehnert, S. *Biomolecular Action of Ionizing Radiation*; CRC Press, 2007.

(3) Han, W.; Yu, K. Ionizing radiation, DNA double strand break and mutation. *Adv. Gene. Res.* **2010**, *4*, 197−210.

(4) Schlumpberger, S.; Lu, N. B.; Suss, M. E.; Bazant, M. Z. Scalable and continuous water deionization by shock electrodialysis. *Environ. Sci. Technol. Lett.* **2015**, *2*, 367−372.

(5) Deng, D.; Dydek, E. V.; Han, J.-H.; Schlumpberger, S.; Mani, A.; Zaltzman, B.; Bazant, M. Z. Overlimiting current and shock electrodialysis in porous media. *Langmuir* **2013**, *29*, 16167−16177.

(6) Deng, D.; Aouad, W.; Braff, W. A.; Schlumpberger, S.; Suss, M. E.; Bazant, M. Z. Water purification by shock electrodialysis: Deionization, filtration, separation, and disinfection. *Desalination* **2015**, *357*, 77−83.

(7) Bazant, M. Z.; Dydek, E. V.; Deng, D.; Mani, A. Method and apparatus for desalination and purification. U.S. Patent 8,801,910 B2, 2014.

(8) Bazant, M. Z.; Dydek, E. V.; Deng, D.; Mani, A. Desalination and purification system. U.S. Patent 8,999,132 B2, 2015.

(9) Mani, A.; Bazant, M. Z. Deionization shocks in microstructures. *Phys. Rev. E: Stat., Nonlinear, Soft Matter Phys.* **2011**, *84*, 061504.

(10) Han, J.-H.; Khoo, E.; Bai, P.; Bazant, M. Z. Over-limiting current and control of dendritic growth by surface conduction in nanopores. *Sci. Rep.* **2014**, *4*, 7056.

(11) Han, J.-H.; Wang, M.; Bai, P.; Brushett, F. R.; Bazant, M. Z. Dendrite suppression by shock electrodeposition in charged porous media. *Sci. Rep.* **2016**, *6*, 28054.

(12) Dydek, E. V.; Zaltzman, B.; Rubinstein, I.; Deng, D.; Mani, A.; Bazant, M. Z. Overlimiting current in a microchannel. *Phys. Rev. Lett.* **2011**, *107*, 118301.

(13) Alizadeh, S.; Bazant, M. Z.; Mani, A. Impact of Network Heterogeneity on Electrokinetic Transport in Porous Media. *J. Colloid Interface Sci.* **2019**, *553*, 451−464.

(14) Nikonenko, V. V.; Kovalenko, A. V.; Urtenov, M. K.; Pismenskaya, N. D.; Han, J.; Sistat, P.; Pourcelly, G. Desalination at overlimiting currents: State-of-the-art and perspectives. *Desalination* **2014**, *342*, 85−106.

(15) Nam, S.; Cho, I.; Heo, J.; Lim, G.; Bazant, M. Z.; Moon, D. J.; Sung, G. Y.; Kim, S. J. Experimental verification of overlimiting current by surface conduction and electro-osmotic flow in micro-channels. *Phys. Rev. Lett.* **2015**, *114*, 114501.

(16) Mani, A.; Zangle, T. A.; Santiago, J. G. On the Propagation of Concentration Polarization from Microchannel−Nanochannel Interfaces Part I: Analytical Model and Characteristic Analysis. *Langmuir* **2009**, *25*, 3898−3908.

(17) Zangle, T. A.; Mani, A.; Santiago, J. G. On the Propagation of Concentration Polarization from Microchannel−Nanochannel Interfaces Part II: Numerical and Experimental Study. *Langmuir* **2009**, *25*, 3909−3916.

(18) Zangle, T. A.; Mani, A.; Santiago, J. G. Theory and experiments of concentration polarization and ion focusing at microchannel and nanochannel interfaces. *Chem. Soc. Rev.* **2010**, *39*, 1014−1035.

DOI: 10.1021/acs.est.9b05380
Environ. Sci. Technol. 2020, 54, 527−536

(19) Conforti, K. M.; Bazant, M. Z. Continuous ion-selective separations by shock electrodialysis. *AIChE J.* **2019**, *66*, No. e16751.
(20) Rana, D.; Matsuura, T.; Kassim, M. A.; Ismail, A. F. Radioactive decontamination of water by membrane processes - A review. *Desalination* **2013**, *321*, 77−92.
(21) Kaur, M.; Zhang, H.; Martin, L.; Todd, T.; Qiang, Y. Conjugates of Magnetic Nanoparticle-Actinide Specific Chelator for Radioactive Waste Separation. *Environ. Sci. Technol.* **2013**, *47*, 11942−11959.
(22) Rahman, R. O. A.; Ibrahium, H. A.; Hung, Y.-T. Liquid radioactive wastes treatment: a review. *Water* **2011**, *3*, 551−565.
(23) Luo, W.; Xiao, G.; Tian, F.; Richardson, J. J.; Wang, Y.; Zhou, J.; Guo, J.; Liao, X.; Shi, B. Engineering robust metal-phenolic network membranes for uranium extraction from seawater. *Energy Environ. Sci.* **2019**, *12*, 607−614.
(24) Sengupta, S. K.; Hooper, E.; Dubost, E. *Processing of Nuclear Power Plant Waste Streams Containing Boric Acid. (Technical Report) 49*; International Atomic Energy Agency, 2019.
(25) Neeb, K.-H. *The Radiochemistry of Nuclear Power Plants with Light Water Reactors*; Walter de Gruyter, 2011.
(26) Park, J.; Chopra, O.; Natesan, K.; Shack, W.; Cullen, W., Jr. Boric acid corrosion of light water reactor pressure vessel materials. *Proceedings of the 12th International Conference on Environmental Degradation of Materials in Nuclear Power System-Water Reactors*, 2005; pp 459−468.
(27) Choo, K.-H.; Kwon, D.-J.; Lee, K.-W.; Choi, S.-J. Selective removal of cobalt species using nanofiltration membranes. *Environ. Sci. Technol.* **2002**, *36*, 1330−1336.
(28) Ashley, N. V.; Roach, D. J. Review of biotechnology applications to nuclear waste treatment. *J. Chem. Technol. Biotechnol.* **1990**, *49*, 381−394.
(29) Pham, T. C. T.; Docao, S.; Hwang, I. C.; Song, M. K.; Choi, D. Y.; Moon, D.; Oleynikov, P.; Yoon, K. B. Capture of iodine and organic iodides using silica zeolites and the semiconductor behaviour of iodine in a silica zeolite. *Energy Environ. Sci.* **2016**, *9*, 1050−1062.
(30) Todd, T. A. *Solvent Extraction Research and Development in the US Fuel Cycle Program*, 2011.
(31) Li, J.; Wang, J. Advances in cement solidification technology for waste radioactive ion exchange resins: A review. *J. Hazard. Mater.* **2006**, *135*, 443−448.
(32) Arar, Ö.; Yüksel, Ü.; Kabay, N.; Yüksel, M. Various applications of electrodeionization (EDI) method for water treatment-A short review. *Desalination* **2014**, *342*, 16−22.
(33) Datta, S. J.; Oleynikov, P.; Moon, W. K.; Ma, Y.; Mayoral, A.; Kim, H.; Dejoie, C.; Song, M. K.; Terasaki, O.; Yoon, K. B. Removal of 90Sr from highly Na+-rich liquid nuclear waste with a layered vanadosilicate. *Energy Environ. Sci.* **2019**, *12*, 1857−1865.
(34) Otte, J. A.; Liebman, D. Method for removing cesium from an aqueous liquid and purifying the reactor coolant in boiling water and pressurized water reactors. U.S. Patent 4,657,731 A, 1987.
(35) Kikuchi, M.; Ga, E.; Funabashi, K.; Yusa, H.; Uchida, S.; Fujita, K. Removal of radioactive cobalt ion in high temperature water using titanium oxide. *Nucl. Eng. Des.* **1979**, *53*, 387−392.
(36) Liu, X.; Wu, J.; Wang, J. Removal of Cs (I) from simulated radioactive wastewater by three forward osmosis membranes. *Chem. Eng. J.* **2018**, *344*, 353−362.
(37) Stoenner, R. W.; Hillman, M. Search for Radiochemical Evidence for Ternary Fission of ^{235}U by Thermal Neutrons. *Phys. Rev.* **1966**, *142*, 716−719.
(38) Sarma, D.; Malliakas, C. D.; Subrahmanyam, K. S.; Islam, S. M.; Kanatzidis, M. G. K2xSn4-xS8-x (x = 0.65−1): a new metal sulfide for rapid and selective removal of Cs+, Sr2+ and UO22+ ions. *Chem. Sci.* **2016**, *7*, 1121−1132.
(39) Cox, B.; Wu, C. Transient effects of lithium hydroxide and boric acid on Zircaloy corrosion. *J. Nucl. Mater.* **1995**, *224*, 169−178.
(40) Min, C. S.; Kun, J. L. *A Study on the Generation of Radioactive Corrosion Product at PWR for Extended Fuel Cycle*, 2001.
(41) Lister, D. H. The Transport of Radioactive Corrosion Products in High-Temperature Water II. The Activation of Isothermal Steel Surfaces. *Nucl. Sci. Eng.* **1976**, *59*, 406−426.
(42) Honda, T.; Minato, A.; Ohsumi, K.; Matsubayashi, H. Radioactive Contamination of Carbon Steel in a Boiling Water Reactor. *Nucl. Technol.* **1984**, *65*, 438−443.
(43) Varga, K.; Hirschberg, G.; Németh, Z.; Myburg, G.; Schunk, J.; Tilky, P. Accumulation of radioactive corrosion products on steel surfaces of VVER-type nuclear reactors. II. 60Co. *J. Nucl. Mater.* **2001**, *298*, 231−238.
(44) Ocken, H. Reducing the Cobalt Inventory in Light Water Reactors. *Nucl. Technol.* **1985**, *68*, 18−28.
(45) Honda, T.; Izumiya, M.; Minato, A.; Ohsumi, K.; Matsubayashi, H. Radiation Buildup on Stainless Steel in a Boiling Water Reactor Environment. *Nucl. Technol.* **1984**, *64*, 35−42.
(46) Khayet, M.; Mengual, J. I.; Zakrzewska-Trznadel, G. Direct contact membrane distillation for nuclear desalination, Part II: experiments with radioactive solutions. *Int. J. Nucl. Desalin.* **2006**, *2*, 56−73.
(47) Park, S.-M.; Park, J.-K.; Kim, J.-B.; Shin, S.-W.; Lee, M.-C. Development of the pilot system for radioactive laundry waste treatment using UV photo-oxidation process and reverse osmosis membrane. *Nucl. Eng. Technol.* **1999**, *31*, 506−511.
(48) Nam, S. H.; Masamba, W. R. L.; Montaser, A. Investigation of helium inductively coupled plasma-mass spectrometry for the detection of metals and nonmetals in aqueous solutions. *Anal. Chem.* **1993**, *65*, 2784−2790.
(49) U.S. Energy Information Administration. Average Price of Electricity to Ultimate Customers by End-Use Sector. https://www.eia.gov/electricity/monthly/epm_table_grapher.php?t=epmt_5_6_a, 2019.
(50) Mitsubishi Heavy Industries, Ltd. US-APWR Design Description. https://www.nrc.gov/docs/ML0630/ML063030474.pdf, 2019.
(51) Ahunbay, M. G.; Tantekin-Ersolmaz, S. B.; Krantz, W. B. Energy optimization of a multistage reverse osmosis process for seawater desalination. *Desalination* **2018**, *429*, 1−11.
(52) Zhu, A.; Christofides, P. D.; Cohen, Y. Minimization of energy consumption for a two-pass membrane desalination: effect of energy recovery, membrane rejection and retentate recycling. *J. Membr. Sci.* **2009**, *339*, 126−137.
(53) Alkhadra, M. A.; Gao, T.; Conforti, K. M.; Tian, H.; Bazant, M. Z. Small-scale desalination of seawater by shock electrodialysis. *Desalination* **2020**, *476*, 114219.
(54) U.S. Government. Accountability Office, Managing Critical Isotopes: Stewardship of Lithium-7 Is Needed to Ensure a Stable Supply. http://www.gao.gov/products/gao-13-716, 2013.
(55) Singh, K.; Bouwmeester, H.; de Smet, L.; Bazant, M.; Biesheuvel, P. Theory of water desalination with intercalation materials. *Phys. Rev. Appl.* **2018**, *9*, 064036.
(56) Zhang, C.; He, D.; Ma, J.; Tang, W.; Waite, T. D. Faradaic reactions in capacitive deionization (CDI) - problems and possibilities: A review. *Water Res.* **2018**, *128*, 314−330.
(57) He, L.; Xu, W.; Song, Y.; Luo, Y.; Liu, X.; Zhao, Z. New Insights into the Application of Lithium-Ion Battery Materials: Selective Extraction of Lithium from Brines via a Rocking-Chair Lithium-Ion Battery System. *Glob. Challenges* **2018**, *2*, 1700079.
(58) Lee, D.-H.; Ryu, T.; Shin, J.; Ryu, J. C.; Chung, K.-S.; Kim, Y. H. Selective lithium recovery from aqueous solution using a modified membrane capacitive deionization system. *Hydrometallurgy* **2017**, *173*, 283−288.

DOI: 10.1021/acs.est.9b05380
Environ. Sci. Technol. 2020, 54, 527−536